Controlled nucleation and growth of CdS nanoparticles by turbulent dispersion

Farzaneh Shayeganfar,[1] Leili Javidpour,[1] Nima Taghavinia,[1] M. Reza Rahimi Tabar,[1,2] Muhammad Sahimi,[3,*] and Faezeh Bagheri-Tar[3]

[1]*Department of Physics, Sharif University of Technology, Tehran 11155-9161, Iran*

[2]*Institute of Physics, Carl von Ossietzky University, Oldenburg D-26111, Germany*

[3]*Mork Family Department of Chemical Engineering & Materials Science, University of Southern California, Los Angeles, California 90089-1211, USA*

(Received 12 April 2009; revised manuscript received 23 December 2009; published 8 February 2010)

We propose and test a method for controlling the size of nanoparticles, which plays a fundamental role in their electrical, optical, and mechanical properties. The method utilizes turbulent mixing, and is applicable to the fabrication of any type of nanoparticle that uses a solution environment in the preparation process. We show by well-controlled experiments on the CdS nanoparticles, which are semiconducting materials, that the average size $\langle d \rangle$ of the particles decreases with Reynolds number Re.

DOI: 10.1103/PhysRevE.81.026304 PACS number(s): 47.27.E−, 47.11.Mn, 61.82.Fk, 81.05.Dz

I. INTRODUCTION

The importance of nanoparticles to modern science and technology cannot be overemphasized. Due to their small size and the special properties that such particles are endowed with, their fabrication has been an active area of research for the past decade or so. They are critical to a wide variety of physical and chemical phenomena, including the formation of materials that mimic ionic solids [1–3], the nanoscale equivalent of ionic liquids [4], composite thin films [5] that are used as low-dielectric constant materials, catalysts and membranes [6], and drug-delivery carriers [7]. The properties of nanoparticles depend on their size [1]. Therefore, control over the particle size distribution (PSD) is highly desirable. Indeed, the potential use of any type of nanoparticle can be fully materialized only if one has precise control on the PSD during the fabrication process. Moreover, the mechanical stability of such particles also depends strongly on their size.

The controlled growth of wide band gap II-VI semiconductors (SCs), which include the SC particles at nanosscales [8], is an important problem that, over the past decade, has attracted great attention [9]. The SC nanoparticles possess many desirable properties. Their optical and electronic properties are unique [10] and have given rise to many possible applications in several fields, such as antireflective coatings [11], emitting devices in the yellow or red spectral region [12], biological labels [13], and bioelectronics [14,15]. Among the various II-VI semiconductors, cadmium sulfate, CdS, has a bulk band gap of 2.45 eV. An upward shift of 0.8 eV with respect to the bulk value is observed in 3 nm nanoparticles [10]. Such a large value of the band gap allows light emission between blue and red wavelengths. Other properties of the SC CdS include band gap widening, nonlinear optical effects [16], and enhanced photoluminescence efficiency. In addition, due to such properties, the SC nanoparticles also have applications in solar cells [17], photodetectors, light-emitting diodes, and biological labels [13,18], as well as single-electron transistors [9,12,19,20], thin-film transistors, and many more.

Several methods have been suggested for the fabrication of the SC nanoparticles, including by precipitation in a solid phase [21,22] that uses porous materials as templates [23,24], growth in nanosize micelles [25,26], and precipitation in a liquid phase [27]. In earlier work, reverse micelles or water-in-oil microemulsions were used as the medium for the synthesis of the nanoparticles, because the individual micelles act as reactors or precipitators. The growth mechanism of the CdS nanoparticles in water-in-oil microemulsions was studied by Towey *et al.* [28] and Suzuki *et al.* [29,30]. The formation of the nanoparticles, obtained by mixing two micellized aqueous solutions, was also studied by the Monte Carlo simulations.

In this paper we use the method of growth in a liquid phase or colloidal precipitation, in order to fabricate CdS nanoparticles. Grown in this way, the nanoparticles comprise of an inorganic core, coated with a layer of organic ligand molecules. The capping agent provides electronic and chemical passivation of the surface dangling bonds [31,32], prevents uncontrolled agglomeration of the nanoparticles, and allows one to chemically manipulate them, similar to large molecules with solubility and reactivity that are determined by the identity of the surface ligand. We present a method for the precise control of the nanoparticles' size during their fabrication, which is applicable to the preparation of any nanoparticle that utilizes a solution environment. The method is based on utilizing turbulent mixing in the solution. As we demonstrate below, the method enables us to not only gain deep understanding of the phenomena that happen during the nanoparticles' fabrication, but also control their sizes. In particular, it enables us to reduce both the average and the variance of the PSD by adjusting the Reynolds number Re of the turbulent flow.

The rest of this paper is organized as follows. In the next section we describe the method for the fabrication of the CdS nanoparticles that we study in this paper. Section III describes the results, while Sec. V presents a discussion of the effect of turbulence of the nanoparticles fabrication process. Section V summarizes the paper.

*Corresponding author. moe@iran.usc.edu

 ©2010 The American Physical Society

II. EXPERIMENTAT PROCEDURE

Fabrication of CdSe nanocrystals in nanoliter droplets was reported by Chan *et al.* [33] who utilized a flow-focusing nanojet structure. The method that we utilize is somewhat similar, except that the jet for injecting the solution is not at the nanoscale. We utilize the method of precipitation in a liquid phase. The fabrication process is begun by nucleation in a solution of the nanoparticles that have an inorganic core, proceeds by the particles growth, and ends by coating their surface by a layer of organic ligand molecules. The coating prevents uncontrolled agglomeration of the nanoparticles, allows one to manipulate them chemically, and prevents the dangling bonds on the surface to negatively affect the properties of the particles.

The CdS nanoparticles were formed through a chemical precipitation method. $Cd(NO_3)_2$ and Na_2S with concentrations of 1 and 10 m*M* were used as the reactants, and thioglycerol (TG, $C_3H_5O_2S$) with a concentration of 5 m*M* was added as the capping agent. Typically, 25 ml solution of the reactants and the capping agent was prepared. The experiments are carried out in two separate stages. (1) In preliminary experiments the CdS nanoparticles were synthesized by adding drops of the $Cd(NO_3)_2$ solution into the beaker that contained Na_2S and the TG. As a result of the reaction,

$$Cd(NO_3)_2 + Na_2S \rightarrow CdS + 2Na(NO)_3,$$

the CdS nanoparticles were formed quickly. (2) We then carried out experiments with an injection set up consisting of a stainless steel tube (1 cm internal diameter, 100 cm long) that held the Cd solution, with a hypodermic needle at one end that represented the jet nozzle. The other end of the tube was connected to an air compressor with a pressure between 1–5 bar. The injection tube was placed vertically. The injection creates turbulent mixing in the solution. The injection velocity was estimated by measuring the drain time, considering the geometrical factors, and the Reynolds number was calculated using the value of injection velocity [34].

The velocity v_0, by which the $Cd(NO_3)_2$ solution is injected into the Na_2S+the TG solution, is an important factor that influences the changes in the size of the CdS nanoparticles. If v_0 is high enough, turbulent mixing is generated in the solution in which the nuclei of the CdS particles are forming. The turbulence prevents the small particles from agglomeration. The uv-visible absorption spectroscopy was method of monitoring the growth of the nanoparticles and measuring their size. A Jasco V-530 spectrometer was employed for the uv-visible spectroscopy. The optical absorption of the CdS nanoparticles was measured during the growth process, as were their evolution with a dip probe, connected to a CCD spectrometer (Avaspec 2048 TEC).

III. RESULTS

Extensive experiments were carried out using the procedure described above. In what follows the results are described and discussed.

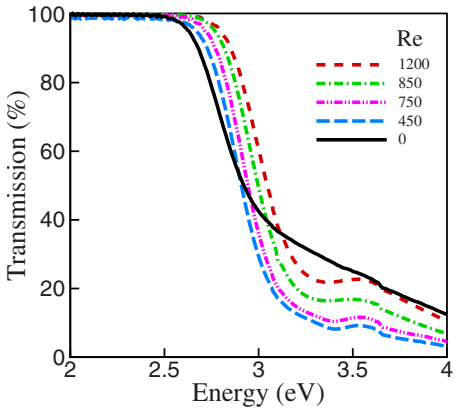

FIG. 1. (Color online) The transmission spectra of the CdS nanoparticles that were formed in the flow with the Reynolds number $\simeq 0$, as well as those with the turbulent jet at various Reynolds numbers.

A. Effect of turbulence on nanoparticles' size

Figure 1 presents the transmission spectra for the sample prepared with a very slow flow system with, $Re \simeq 0$. The band gap energy in this step is 2.78 eV. The band gaps obtained from the spectra were used to estimate the nanoparticles' size using the semiempirical relation of Lippens and Lannoo [35] that relates the size of the CdS particles to the band gap values. Such estimates are referred to as the *optical sizes*. The predictions of the semiempirical relation agree well with the tight-binding calculations for the smaller particle sizes [35], and with the effective-mass approximation (EMA) [31,36,37] for the larger ones. The EMA has been shown to slightly overestimate the actual size obtained from transmission electron microscopy [32].

The optical size remains an accurate and easy-to-obtain indication of the nanoparticles' growth process. Increasing the injection velocity of $Cd(NO_3)_2$ influences its diffusion coefficient and, consequently, decreases the size of the CdS nanoparticles. This is due to the turbulence being an impediment to the particles sticking together. The transmission spectra for samples prepared in different Reynolds number are also shown in Fig. 1.

Figure 2 presents the results of the experiments that were performed at various injection velocities. As seen clearly, the

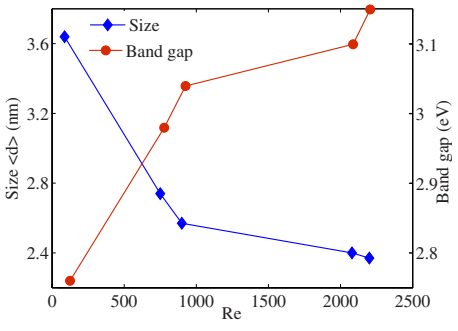

FIG. 2. (Color online) Dependence of the band gap and the mean optical size of the CdS nanoparticles in the solution on the Reynolds number Re.

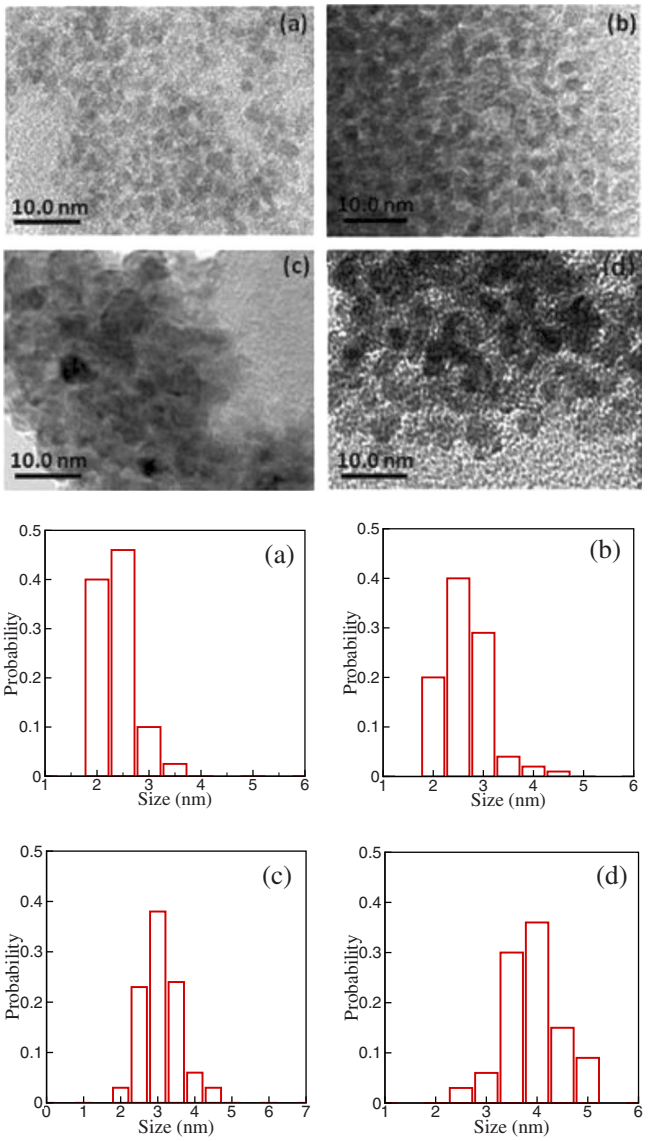

FIG. 3. (Color online) TEM images and the corresponding size distributions of the CdS nanoparticles, fabricated at four Reynolds numbers. (a) Re=2300, (b) Re=900, (c) Re=640, and (d) Re≃0.

band gap of the particles increases as their size decreases, which is due to the increase in the flow velocity by which $Cd(NO_3)_2$ flows into the system that contains the initial solution. The experiments were then repeated for several Reynolds numbers of the flow, defined as, $\mathrm{Re}=v_0 D/\mu$, where v_0, D, and μ are, respectively, the injection velocity, diameter of the injection needle, and the average viscosity of the fluid.

In addition, we used transmission electron microscopy (TEM) images and x-ray diffraction (XRD) patterns to study the uniformity of the particles produced, and measure their final average sizes and their variances. We used a JEOL JEM 2100 LaB6 microscope at a voltage of 200 kV, with a scanning time of about 1 s. An ultrathin carbon sample (Ted Pella, Inc., California), supported by a lacey carbon film on a 400 mesh copper grid, was utilized. Figure 3 shows the TEM images of the CdS nanoparticles, fabricated at four Reynolds numbers, together with the corresponding PSDs. They indicate that relatively uniform particle sizes, i.e., narrow PSDs,

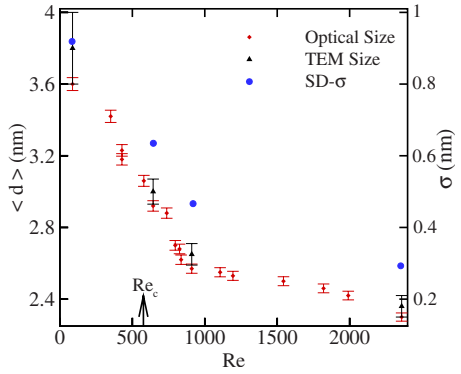

FIG. 4. (Color online) Dependence of the average size $\langle d\rangle$ of the nanoparticles on the Reynolds number Re, black triangle symbols are TEM measurements. Arrow indicates the critical value Re_c of the Reynolds number at which a turbulent jet appears.

are obtained at high Reynolds numbers Re. But, as the Re decreases, the PSD becomes broader. A previous TEM study of CdS nanoparticles [38] presented very similar TEM images, and had reached the same conclusion.

The TEM images are digitized. The PSD was constructed by counting the number of pixels for each particle in each image. For each Reynolds numbers we used six TEM images. Then, the average and variance of the PSD were estimated. Figure 4 presents the change in the nanoparticles' final (after saturation) average size and their standard deviation as a function of the Reynolds number.

As the data demonstrate, increasing the Re decreases the size of the nanoparticles from 3.6 nm at low Re to 2.3 nm at high Re. In the experiments the critical Reynolds number Re_c at which a turbulent jet appears is about 600. As shown in Fig. 4, there appear to be two regimes for the average size of the particles, one for low to moderate and a second one for high values of the Re. In the first regime the average size $\langle d\rangle$ of the nanoparticles appears to decrease roughly as

$$\langle d\rangle \propto a - b\ \mathrm{Re}, \tag{1}$$

where $a \simeq 3.91$ and $b \simeq 1.5\times 10^{-3}$, respectively. There is a crossover in the dependence of $\langle d\rangle$ on Re at which the linear behavior changes to a quadratic regime. The crossover occurs at about $\mathrm{Re}\simeq 900$, relatively close to the critical Reynolds number at which the turbulent jet appears.

Also shown in Fig. 4 is the standard deviation σ of the particles' sizes and its dependence on the Reynolds number. σ was estimated using the TEM images and the distributions shown in Fig. 3. The standard deviations are given by σ_s/N, where σ_s is the standard deviation of the PSD and N is the number of TEM images used in constructing the PSD. Moreover, Fig. 4 also indicates that the estimated average size of the particles from the optical method underestimates the actual sizes that we determined from the TEM images.

Figure 5 presents the XRD spectra of the same samples, where the nanoparticles had been extracted from the solutions. The XRD data provide information on the crystalline phase of the nanoparticles, as well as their size. The diffraction peaks are broad, confirming that the crystallites are nanosized. The maximum of the first peak (at about 28°)

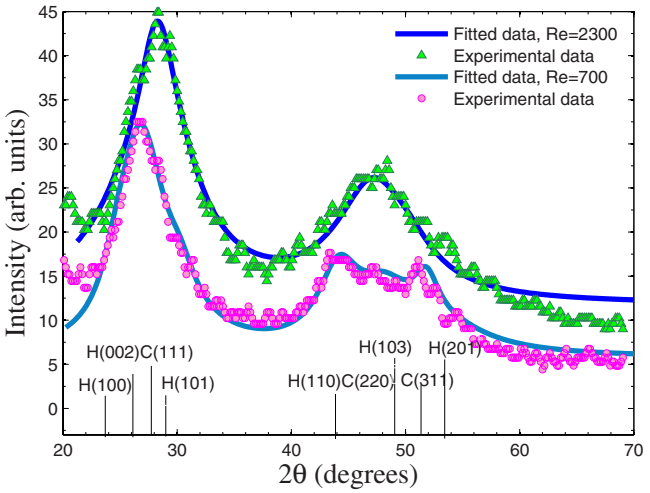

FIG. 5. (Color online) The XRD spectra for the CdS nanoparticles, fabricated at two Reynolds numbers Re. The size of the nanoparticles obtained from the width of peaks is also shown.

shifts slightly to lower angles as the Reynolds number decreases from 2300 to 700. The second peak (at about 48°) is resolved to two peaks at Re=700. Since there are two main peaks for the hexagonal phase of CdS at 28.3° and 48.1° [corresponding to the (101) and (103) planes], and three main peaks for the cubic phase at 26.5°, 43.9°, and 51.9° [corresponding to the (111), (220), and (311) planes], one may conclude that the high-Re samples contain the hexagonal phase, whereas the cubic phase is present in the low-Re samples, consistent with the previous studies that indicated that the CdS particles possess both the hexagonal and cubic phases in the nanosize regime [39–41].

In many cases the two phases cannot be resolved, due to the similarity of their peaks and the fact that the broad peaks appear for nanocrystalline CdS. In our experiments, however, the phases are relatively resolvable and, as a result, one obtains a shift of the phase from hexagonal to cubic when the Reynolds number is lowered. To make the last claim more quantitative, we fitted the XRD data using the Lorenz peak functions at the positions of the cubic and hexagonal peaks, and with the relative peak intensities reported in the JCPDS database (for the XRD experiments). The parameters for the fitting were the background level, the peaks' widths, and the intensity of the 26.5° and 28.3° peaks that correspond to the cubic and hexagonal phases. Typical results are illustrated for the case of Re=700 in Fig. 6. The background was omitted to separate the curves representing the fitted peaks from the actual data.

The results of the fit are summarized in Table I. The second column of Table I presents the percentage of the hexagonal phase in the solution, which was estimated using the intensity of the highest peaks of the hexagonal and cubic phases, and is an indication of the true volume percentage of the two phases. Observe that the volume fraction of the hexagonal phase decreases as the Reynolds number does. Table I also presents the calculated XRD sizes for the nanoparticles. They were computed using the peaks' widths obtained from the fittings, together with the Scherer equation [42],

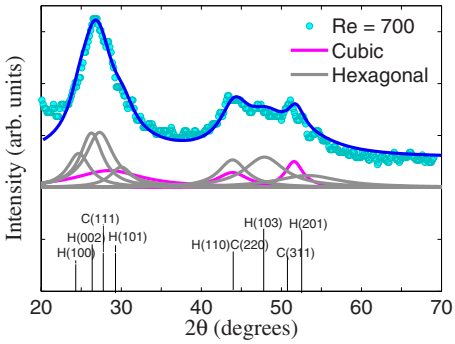

FIG. 6. (Color online) Fit of a typical XRD pattern. The peak components of the fitted curve are shown below the pattern, as are the positions of the cubic and hexagonal phases.

$$\langle d \rangle = \frac{k\lambda}{\beta \cos \theta}, \tag{2}$$

where k is the shape factor (taken to be 1), β is the full-width half-maximum, λ is the x-ray wavelength of the radiation, and θ is the Brag angle. The XRD-based sizes are also compared with the optical sizes in Table I. While they increase with the Reynolds number (as they should), their values are about 13% smaller than the corresponding optical sizes.

B. Dynamics of the nanoparticle growth

Also investigated was the dynamics of the growth of the CdS nanoparticles, with the goal of understanding its mechanism. Figure 7(a) presents the optical transmission spectra for the CdS nanoparticles over the times 3–30 s. The band gap changes considerably over the time period. The trends in the band gap changes may then be converted into the corresponding variations in the nanoparticles' sizes. Figure 7(b) depicts the absorption coefficients of the solutions. The height of the shoulder of the absorption curves is a qualitative measure of the total mass of the CdS nanoparticles grown in the solution. The relative concentration of the grown CdS particles in the solution may also be obtained from the optical transmission spectra, using the height of the band edge shoulder. According to the Beer-Lambert law [43], $\alpha = -\log(\mathcal{T})$ (where $\mathcal{T}$ is the transmission) is proportional to the concentration of the light absorbing species, i.e., the CdS particles. As an approximation, we assume that the changes in the particle size make no discernable change in the oscillator strength of the band gap transition.

The values of the concentration during the growth process are also displayed in Fig. 8(a). One notes that the CdS concentration also increases with time for about 30 s and then

TABLE I. Variations of the crystalline phase, the XRD, and the optical sizes as a function of the Reynolds number Re.

Re	Hexagonal (percentage)	XRD size (nm)	Optical size (nm)
2300	100	2.0	2.3
700	57	2.64	2.91

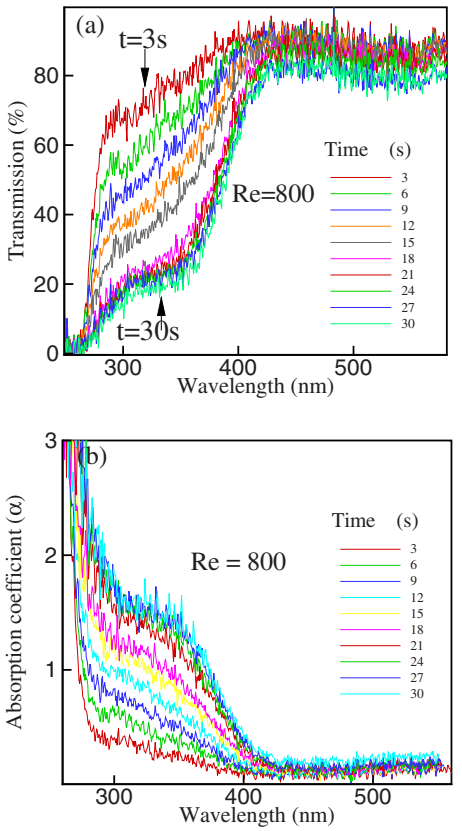

FIG. 7. (Color online) (a) Time dependence of the transmission spectra on wavelength. (b) Change of the absorption spectra as the reaction (time) proceeds.

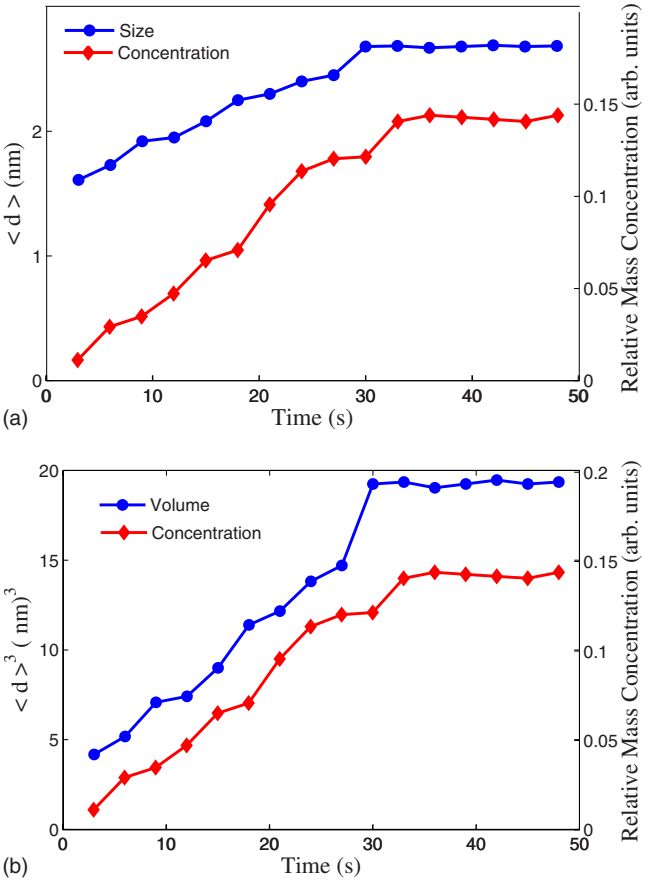

FIG. 8. (Color online) (a) Time dependence of the nanoparticles' average size $\langle d \rangle$ and their concentrations at the Reynolds number, Re=800. (b) The nanoparticles' average volume and concentrations at the same Re as in (a).

saturates. The trend is similar to the changes in the particle size. An important finding here is that the concentration (C) at all times is proportional to the volume of nanoparticles, $\langle d \rangle^3$, where $\langle d \rangle$ is the average size of nanoparticles. This is illustrated in Fig. 8(b), where both quantities are plotted in the same graph. This demonstrates that the growth during the injection time proceeds through the growth of individual nanoparticles, and is the result of the high supersaturation during the injection. Monodispersed growth requires independent growth of the particles without mass transfer *between* the particles.

Figure 9 presents the time dependence of the average size of the CdS nanoparticles for several Reynolds number Re. At the beginning of the reaction, the growth of CdS is fast, but after a while the average particle size saturates and its growth stops. Moreover, saturation of the CdS' size happens more rapidly at high Reynolds numbers and, therefore, their size is smaller at such values of the Re than those at low Re.

It is also instructive to see how the average number $\langle N \rangle$ of the CdS particles varies with the time, as well as the Reynolds number Re. Experimental data for $\langle N \rangle$ are shown in Fig. 10(a) for two Reynolds numbers. The results show that flow with a higher Re results in higher $\langle N \rangle$, since it prevents the growth of the smaller particles by coagulation. Experimental results for the final number $\langle N_f \rangle$ of the CdS particles (after it reaches saturation) are shown in Fig. 10(b).

IV. EFFECT OF TURBULENT MIXING

It has been a considerable experimental, theoretical, and computational challenge for several decades to capture and represent turbulent mixing that, in high-Reynolds-number flows, occurs across a spectrum of a wide span of scales. It is now well known that turbulent mixing is a multiscale phenomenon in which the macroscale fluctuations affect micro-

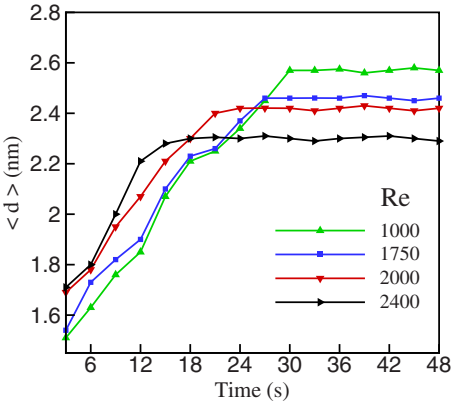

FIG. 9. (Color online) (a) Evolution of the average size of the nanoparticles for different Reynolds number Re.

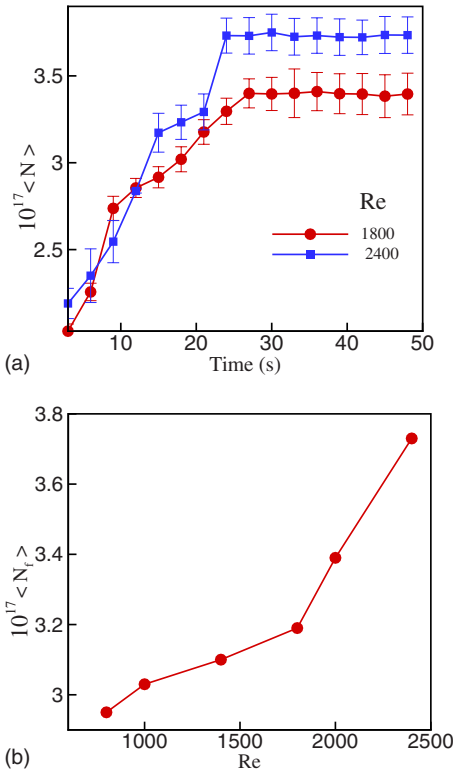

FIG. 10. (Color online) (a) Evolution of the average number of the CdS nanoparticles and its dependence on time. (b) The measured dependence of the final (saturated) number of the CdS nanoparticles on the Re.

scale features. A fluid entrained, or introduced in a turbulent region, is transported and dispersed across it by the motions that are induced by the largest to the smallest eddies. High-Reynolds-number turbulent flows generate large interfacial surface area that permits the slow molecular mixing to proceed efficiently. Turbulent mixing may be viewed as a three-stage process [44] of entrainment, dispersion, and diffusion that span the entire spectra of time and space scales of the flow.

In the simplest case mixing is passive and does not change the dynamics of turbulent fluid. This is usually called level-1 mixing. Level-2 mixing is coupled to the flow dynamics, as in mixing of fluids with different densities in an acceleration or gravitational field, such as the Rayleigh-Taylor [45] and Richtmyer-Meshkov [34] instabilities. Level-3 mixing produces changes to the fluids, e.g., in their compositions, densities, etc., which in turn are coupled to the dynamics (see [46–48] for reviews of fluid turbulence). Because of very low molar concentration of the Cd^{2+} and CdS nanoparticles, we may safely assume that the mixing in our experiments is a passive mixing.

As pointed out above, the nanoparticles grow by two mechanisms: by picking up the non-nucleated product molecules, and by coagulation of the small nanoparticles. The initial growth of the nanoparticles is primarily through picking up the non-nucleated product molecules, because the probability of collision between the two reactants is high. After all, or nearly all, the reactants have been consumed to form the particles, coagulation is the only mechanism that allows them to grow further. Therefore, if the surface that separates the two ions or mixing layers is large enough, then CdS nucleation will take place on the surface (A) far from the two ions. Hence, the number of the CdS nucleation increases. As a result of the small particles being created, if the surface (A) is small, the distance between the CdS nucleations will be very small and will cause the coagulation of the nanoparticles.

An important and practical tool of decreasing the nanoparticles' size is the injection velocity v_0 of $Cd(NO_3)_2$. If v_0 is large enough, the number of the Cd^{2+} ions per unit time that enter the system will be large. At the same, large injection velocities v_0 help mix the Cd^{2+} and S^{2-} ions faster. Therefore, large values of v_0 increase the effective surface (A) and create small nanoparticles, whereas with values of v_0 the diffusion of the Cd^{2+} ions and formation of the CdS nanoparticles are slow. In that case, the probability of aggregation of the CdS nanoparticles for generating the $(CdS)_n$ clusters increases.

The question may arise as to why turbulence should affect processes and particles on the nanometer scale. To address this issue one must estimate the smallest turbulent scales that form in the flow. Hence, let us determine the important length scales in the experiments. Because of the ionic nature of the solutions in the experiments, the Debye length scale λ_D for an electrolyte or a colloidal dispersion should be estimated. It is given by [49]

$$\lambda_D = \sqrt{\frac{\epsilon_0 \epsilon_r k_B T}{2 N_A I e^2}}, \tag{3}$$

where I is the ionic strength of the electrolyte with its unit being mole/m^3, and is given by the usual expression,

$$I = \frac{1}{2}\sum_{i=1}^{n} C_i Z_i^2. \tag{4}$$

Here, C_i is the molar concentration of the ionic solutions, Z_i is the charge number of the ions, ϵ_0 is the permittivity of free space, $\sim 8.854 \times 10^{-12}$ $C^2(Jm)^{-1}$, ϵ_r is the relative permittivity of the CdS particles, which is equal to 5.7, k_B is the Boltzmann's constant, 1.38×10^{23} J/k, T is the temperature (here, 300 K), N_A is the Avogadro number, 6.02×10^{23}, and e is the elementary charge, 1.602×10^{-19} C. Thus, the Debye length in the experiments is about, $\lambda_D \simeq 258$ nm.

Another relevant length scale is the average dissipation scale η, which is estimated using the diameter D of the needle and the Reynolds number as, $\eta = D\,\mathrm{Re}^{-3/4}$. For Re $=2400$ and $D=0.1$ mm, the dissipation scale is $\eta \simeq 300$ nm. The dissipation scale η has a distribution $Q(\eta)$ given by [50]

$$Q(\eta) = \frac{1}{\pi\eta[b\,\log(L/\eta)]^{1/2}} \int_{-\infty}^{\infty} dx \times \exp\left\{ -x^2 - \frac{[\log(\sqrt{2}x\,\mathrm{Re}_L(\eta/L)^{a+1})]^2}{4b\,\log(L/\eta)} \right\}, \tag{5}$$

where $a \simeq 0.383$, $b \simeq 0.0166$, and L is the integral length scale of the turbulence. Close to $\eta \simeq 300$ nm, the dissipation

scales follow the distribution (5) and, therefore, for a given Reynolds number there is a nonzero probability of having, $\eta \simeq \lambda_D$. This explains why turbulence influences the process at the nanoscale.

Thus, we may summarize the entire process as follows. Turbulence gives rise to an effective turbulent diffusivity, which is usually much larger than the molecular diffusivity and help the Cd particles to reach the S^{2-} ions quickly. In high-Re flows, however, the particles convection also plays an important role, because the large-scale fluctuations make rapid mixing possible. Therefore, the total turbulent dispersion is the sum of the molecular diffusion (which may be small), turbulent diffusion, and shear dispersion. In our experiments the critical Reynolds number for this to be effective is about 600. Thus, in the experiments at high Re the process is a turbulent diffusion-controlled reaction.

V. SUMMARY

It was demonstrated that the size of the CdS nanoparticles can be controlled by turbulent mixing. The optical size of the particles was shown to decrease with increasing the Reynolds numbers. Also studied was the dynamical growth of the CdS nanoparticles. The growth in the solution occurs via two mechanisms. In one a CdS particle grows by picking up the available S^{2-} ions. In the second mechanism a CdS particle grows by coagulation with other CdS particles. The size of the nanoparticles eventually saturates, as their concentration increases. We also demonstrated through the TEM images that the particle size distribution is narrower at higher injection velocities or higher Reynolds numbers.

To gain a deeper understanding of the phenomena reported here, we have carried out molecular dynamics simulations of the processes. The results will be reported elsewhere [51].

ACKNOWLEDGMENTS

The TEM experiments were carried at the Dohney Eye Institute of the University of Southern California. Work at USC was supported in part by the National Science Foundation.

[1] H. Gleiter, Acta Mater. **48**, 1 (2000).
[2] G. A. DeVries, M. Brunnbaer, Y. Hu, A. M. Jackson, B. Long, B. T. Neltner, O. Uzum, B. H. Wunsch, and F. Stellacci, Science **315**, 358 (2007).
[3] E. V. Shevchenko, D. V. Talapin, N. A. Kotov, S. O'Brien, and C. B. Murray, Nature (London) **439**, 55 (2006).
[4] A. B. Bourlinos, E. P. Giannelis, Q. Zhang, L. A. Archer, G. Floudas, and G. Fytas, Eur. Phys. J. E **20**, 109 (2006).
[5] E. Nedaee Oskoee and M. Sahimi, Phys. Rev. B **74**, 045413 (2006).
[6] F. Bagheri-Tar, M. Sahimi, and T. T. Tsotsis, Ind. Eng. Chem. Res. **46**, 3348 (2007).
[7] R. S. Langer, Science **293**, 58 (2001).
[8] T. Di Luccio, A. M. Laera, L. Tapfer, S. Kempter, R. Kraus, and B. Nickel, J. Phys. Chem. B **110**, 12603 (2006).
[9] A. P. Alivisatos, Science **271**, 933 (1996).
[10] R. Rossetti, L. Ellison, J. M. Gibson, and L. E. J. Brus, J. Chem. Phys. **80**, 4464 (1984); R. Rossetti, R. Huli, J. M. Gibson, and L. E. J. Brus, *ibid.* **82**, 552 (1985).
[11] J. H. Park, J. Y. Kim, B. G. Chin, Y. C. Kim, and O. O. Park, Nanotechnology **15**, 1217 (2004).
[12] V. L. Colvin, M. C. Schlamp, and A. P. Alivisatos, Nature (London) **370**, 354 (1994).
[13] M. Bruchez, Jr., M. Moronne, P. Gin, S. Weiss, and A. P. Alivisatos, Science **281**, 2013 (1998).
[14] E. Katz and I. Willner, in *Nanobiotechnology*, edited by C. M. Niemeyer and C. A. Mirkin (Culinary and Hospitality Industry Publications, Houston, 2004), Chap. 14.
[15] I. Willner and B. Willner, Pure Appl. Chem. **74**, 1773 (2002).
[16] M. Sahimi, *Heterogeneous Materials II* (Springer, New York, 2003), Chap. 3.
[17] R. S. Singh, V. K. Rangari, S. Sanagapalli, V. Jayaraman, S. Mahendra, and V. P. Singh, Sol. Energy Mater. Sol. Cells **82**, 315 (2004).
[18] W. J. Parak, D. Gerion, T. Pellegrino, D. Zanchet, C. Micheel, S. C. Williams, R. Boudreau, M. A. Le Gros, C. A. Larabell, and A. P. Alivisatos, Nanotechnology **14**, R15 (2003).
[19] D. L. Klein, R. Roth, A. K. L. Lim, A. P. Alivisatos, and P. L. McEuen, Nature (London) **389**, 699 (1997).
[20] B. A. Ridley, B. Nivi, and J. M. Jacobson, Science **286**, 746 (1999).
[21] T. M. Hayes, L. B. Lurio, J. Pant, and P. D. Persans, Solid State Commun. **117**, 627 (2001).
[22] W. Wang, Z. Liu, C. Zheng, C. Xu, Y. Liu, and G. Wang, Mater. Lett. **57**, 2755 (2003).
[23] Y. Shan, L. Gao, and S. Zheng, Mater. Chem. Phys. **88**, 192 (2004).
[24] F. Gao, Q. Lu, and D. Zhao, Chem. Phys. Lett. **360**, 585 (2002).
[25] A. R. Kortan, R. Hall, R. L. Opila, M. G. Bawendi, M. L. Steigerwald, P. J. Carroll, and L. E. Brus, J. Am. Chem. Soc. **112**, 1327 (1990).
[26] B. Liu, G. Q. Xu, L. M. Gan, C. H. Chew, and W. S. Li, J. Appl. Phys. **89**, 1059 (2001).
[27] S. Wageh, Z. S. Ling, and X. Xu-Rong, J. Cryst. Growth **255**, 332 (2003).
[28] T. F. Towey, A. Khan-Lodhi, and B. H. Robinson, J. Chem. Soc., Faraday Trans. **86**, 3757 (1990).
[29] K. Suzuki, M. Harada, and A. Shioi, J. Chem. Eng. Jpn. **33**, 3262 (1996).
[30] K. Suzuki, N. Mizutani, and M. Harada, J. Chem. Eng. Jpn **32**, 31 (1999).
[31] Y. Kayanuma, Solid State Commun. **59**, 405 (1986).
[32] M. Marandi, N. Taghavinia, A. Irajizad, and S. M. Mahdavi, Nanotechnology **16**, 334 (2005).
[33] E. M. Chan, A. P. Alivisatos, and R. A. Mathies, J. Am. Chem. Soc. **127**, 13854 (2005).
[34] The shape of the turbulent jet that is formed in the experiments

is very much similar to those in the experiments on turbulent mixing, as described by P. E. Dimotakis, Annu. Rev. Fluid Mech. **37**, 329 (2005), Fig. 2.
[35] P. E. Lippens and M. Lannoo, Phys. Rev. B **39**, 10935 (1989).
[36] E. Brus, J. Chem. Phys. **79**, 5566 (1983); **80**, 4403 (1984).
[37] S. V. Nair, S. Sinha, and K. C. Rustagi, Phys. Rev. B **35**, 4098 (1987).
[38] Y. Ni, X. Ge, H. Liu, X. Xu, and Z. Zhang, Radiat. Phys. Chem. **61**, 61 (2001).
[39] P. M. A. Farias, B. S. Santos, R. L. Longo, R. Ferreira, and C. L. Cesar, Mater. Chem. Phys. **89**, 21 (2005).
[40] Y. J. Yang and B. J. Xiang, J. Cryst. Growth **284**, 453 (2005).
[41] J. Lee, Thin Solid Films **451-452**, 170 (2004).
[42] M. Winterer, in *Nanocrystalline Ceramics: Synthesis and Structure*, edited by R. Hull, R. M. Osgood, Jr., and J. Parisi (Springer, Berlin, 2002), p. 21.
[43] J. D. J. Ingle and S. R. Crouch, *Spectrochemical Analysis* (Prentice Hall, New Jersey, 1988).
[44] C. Eckart, J. Mar. Res. **VII**, 265 (1948).
[45] S. Chandrasekhar, *Hydrodynamic and Hydromagnetic Stability*, 3rd ed. (Oxford University Press, London, 1970).
[46] A. S. Monin and A. M. Yaglom, *Statistical Fluid Mechanics: Mechanics of Turbulence* (MIT Press, Cambridge, 1975), Vol. 2.
[47] U. Frisch, *Turbulence, The Legacy of A. N. Kolmogorov* (Cambridge University Press, Cambridge, England, 1995).
[48] A. Tsinober, *An Informal Introduction to Turbulence* (Kluwer, Dordchet, 2001).
[49] W. B. Russel, D. A. Saville, and W. R. Schowalter, *Colloidal Dispersions* (Cambridge University Press, London, 1989).
[50] S. C. C. Bailey, M. Hultmark, J. Schumacher, V. Yakhot, and A. J. Smits, Phys. Rev. Lett. **103**, 014502 (2009).
[51] L. Javidpour, F. Shayeganfar, M. R. Rahimi Tabar, M. Sahimi, and N. Taghavinia, Phys. Rev. E (to be published).